

Article

Modified Maximum Likelihood Estimation Metal Magnetic Memory Quantitative Identifying Model of Weld Defect Levels Based on Dempster–Shafer Theory

Haiyan Xing ^{1,*}, Cheng Xu ^{1,2}, Ming Yi ¹, Shenrou Gao ^{1,2} and Weinan Liu ¹

¹ School of Mechanical Science and Engineering, Northeast Petroleum University, Daqing 163318, China; xucheng1357@163.com (C.X.); 15765967060@163.com (M.Y.); gaoshenrou@163.com (S.G.); 8338773269@163.com (W.L.)

² School of Mechanical and Electronic Engineering, Qiqihar University, Qiqihar 161006, China

* Correspondence: xxhyyhit@163.com

Abstract: Metal magnetic memory (MMM) is a nondestructive testing technology based on the magnetomechanical effect, which is widely used in the qualitative detection of stress concentration zones for welded joints. However, there is inevitable residual stress after welding, which brings the bottleneck of quantitative identification between the weld residual stress concentration and the early hidden damage. In order to overcome the bottleneck of quantitative identification of weld defect levels with MMM technology, a modified maximum likelihood estimation (MLE) MMM quantitative identifying model is first proposed. The experimental materials are Q235B welded plate specimens. Fatigue tension experiments were operated to find the MMM feature laws of critical hidden crack by comparing with synchronous X-ray detection results. Six MMM characteristic parameters, which are, $\Delta H_p(x)$, G_x^{\max} , Z_x^{\max} , $\Delta H_p(y)$, G_y^{\max} and Z_y^{\max} , are extracted corresponding to the normal state, the hidden crack state and the macroscopic crack, respectively. The MLE values of the six parameters are obtained by the kernel density functions with optimized bandwidth from the view of mathematical statistics. Furthermore, the modified MLE MMM quantitative identifying model is established based on D–S theory to overcome the partial overlap of MLE values among different defect levels, of which the uncertainty is as low as 0.3%. The verification result from scanning electron microscopy (SEM) is consistent with the prediction of the modified MLE MMM model, which provides a new method for quantitative identification of weld defect levels.

Keywords: metal magnetic memory; defect levels; welded joints; maximum likelihood estimation; D–S theory



Citation: Xing, H.; Xu, C.; Yi, M.; Gao, S.; Liu, W. Modified Maximum Likelihood Estimation Metal Magnetic Memory Quantitative Identifying Model of Weld Defect Levels Based on Dempster–Shafer Theory. *Appl. Sci.* **2023**, *13*, 7959. <https://doi.org/10.3390/app13137959>

Academic Editors: Dong Wang, Shiqian Chen and Siliang Lu

Received: 30 May 2023

Revised: 4 July 2023

Accepted: 5 July 2023

Published: 7 July 2023



Copyright: © 2023 by the authors. Licensee MDPI, Basel, Switzerland. This article is an open access article distributed under the terms and conditions of the Creative Commons Attribution (CC BY) license (<https://creativecommons.org/licenses/by/4.0/>).

1. Introduction

Welded joints always work in high temperature, high pressure and corrosive environments, which are prone to cause cracks, fractures and explosions after long-time operation [1]. For this reason, the testing and evaluation of welded joints are very important for pressure vessels, piping and other equipment in service. Principally, it is necessary to identify the early critical state of hidden cracks because accidents caused by hidden cracks may occur at any time [2]. However, the stress concentration zones (SCZs) and early hidden cracks can not be found by traditional nondestructive testing (NDT), such as ultrasonic testing, X-ray inspect and eddy current testing, until the macroscopic crack has been formed [3,4]. A new NDT technology, called metal magnetic memory (MMM) testing, can not only detect macroscopic cracks but also find SCZs and early hidden cracks without any magnetization devices or special treatment for the tested surface [5,6]. Based on the self-magnetization phenomenon of ferromagnetic materials, the MMM magnetic-field intensity H_p is characterized by the polarity varying along the normal component $H_p(y)$ and maximum value along the tangential component $H_p(x)$ on SCZs [7,8].

The appearance of MMM testing brings a great improvement in SCZs and early defect detection. Doubov et al. demonstrated that the natural magnetization can be applied to inspect structural inhomogeneity and residual stresses which formed during the fabrication of ferromagnetic material by the MMM method [9]. Shi et al., established a magnetomechanical model based on a nonlinear constitutive relation, and analyzed the model using the finite element method quantitatively [10]. Avakian et al. presented a constitutive modelling for ferromagnetic materials under multiaxial multifield loading with different boundary conditions, which can predict magnetization, strain and stress [11]. Ni et al. established a damage model represented by MMM characteristics through fatigue experiments of three point bending and developed a fatigue life prediction method based on the relationship of damage parameter and normalized life [12]. Yao evaluated the contact damage of ferromagnetic materials under nonferromagnetic and ferromagnetic indenters by measuring the signals of the magnetic flux leakage [13]. Xu et al. studied the MMM characteristics of buried defects under different load stages and found the strength of the magnetic field and its gradient decrease with the increasing of the burial depth [14]. Liu proposed the contour plot method to visually analyze the size of defects and established a mathematical model of non-uniform magnetic charge for pipeline leak detection. The peak-to-valley spacing and peak-to-valley values in the contour plot of MFL signal can directly reflect the location and size of defects, and the signal eigenvalues follow the trend of first-order decreasing exponential function, and the first-order derivatives of signal eigenvalues show a trend of first decreasing and then increasing with the decrease of mesh size, and the extreme point of the derivative curve is the best mesh size [15,16]. By comparing with the Standard JB4730-2005 of X-ray detection, the authors set up the MMM reliability model and investigated MMM signal characteristics of SCZs for welded joints [17–19].

However, the MMM signals of welded joints often take on fuzzy and uncertainty due to the interruption of welding residual stress [20,21]. This brings the bottleneck of quantitative identification of weld defect levels with MMM technology, especially between the weld residual stress concentration and the early hidden damage. In order to overcome the bottleneck, a modified MLE MMM quantitative identifying model is proposed based on D–S theory from the perspective of mathematical statistics and information fusion. First, the welded specimens made of Q235B steel are tested with MMM method and synchronous X-ray detection for comparison under the fatigue tension loading. Six MMM characteristic parameters are extracted for the normal state, the hidden crack and the macroscopic crack, respectively. Then, the probability density functions of the six MMM characteristic parameters are obtained based on optimized kernel density function, and an MLE MMM model is established for weld defect level identification. Furthermore, the reliability function is established by calculating the proximity of the MLE value of different defect levels considering that in the identification results from the MLE MMM model exist partial overlaps. The D–S decision rules are obtained by allocating and fusing reliability function. Finally, the MLE MMM quantitative identifying model is innovatively presented based on D–S theory. The modified model solves the overlapping and fuzzy problem of different weld defect levels in MMM signal analysis. The proved results show the uncertainty degree is 0.3%, which provides a new idea of MMM quantitative identification of weld defect levels.

2. Experiments

Steel Q235B, widely used in practical engineering, was selected for the base material of welded plate specimens and H08Mn2SiA for the welding wire. The chemical composition and mechanical properties of Steel Q235B are shown in Tables 1 and 2, respectively. The base metal (BM) of each specimen was machined from a single Q235B plate. Then, the V-shaped groove was adopted, and each specimen was welded from the two identical BM plates. The specimen size and testing lines are shown in Figure 1.

Table 1. The chemical composition of experimental material (wt.%).

C	Si	Mn	P	S
≤0.20	≤0.35	≤1.40	≤0.045	≤0.045

Table 2. The mechanical property of experimental material.

Yield Strength σ_s /MPa	Ultimate Strength σ_b /MPa	Percentage Elongation after Fracture δ /%
≥235	370~500	≥26

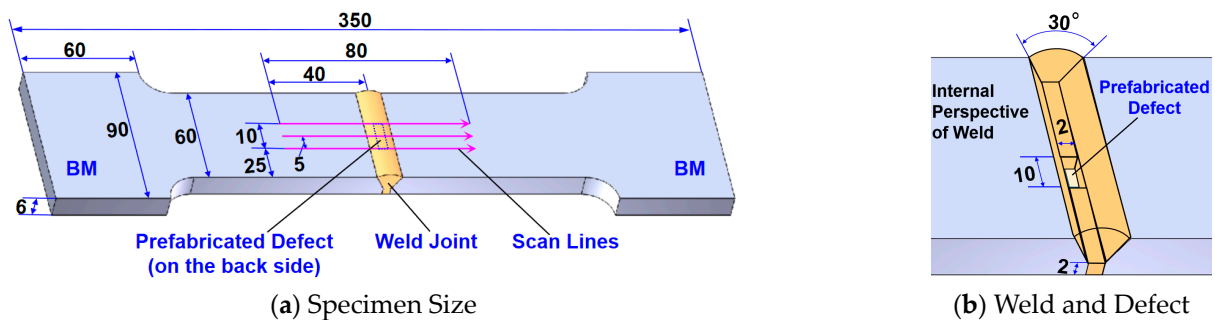


Figure 1. Specimen size and testing lines (in mm).

In order to meet the statistical requirements, 100 specimens were experimented on. The experiments were applied by fatigue tensile loading at room temperature according to the Chinese Standard GB/T 3075-2008 [22]. The maximum tensile stress was 83.3 MPa and the stress ratio was 1/3. In order to control the location of crack initiation and observe its evolution conveniently, the lack of penetration, with a dimension of 10 mm (length) × 2 mm (width) × 2 mm (depth), was prefabricated in the center of each specimen when the argon-arc welding was used for backing. For each experiment, a specimen was randomly selected from 100 specimens for testing. Every 20 kilocycles (kc), the MMM signals were tested by TSC-2M-8 instrument along the longitude and horizontal line L1, L2 and L3, respectively. In order to verify the MMM testing result, the X-ray detection was carried out synchronously.

3. Experiment Results

In Figure 2, the results of X-ray detection show the evolution of fatigue cracks. In Figure 2a, there is only the prefabricated defect without any fatigue cracks, i.e., the normal state. Then, the hidden crack of 1.2 mm was generated after 1280 kc, which has been marked with a circle in Figure 2b and cannot be seen with the naked eye. At last, the macroscopic crack visible to eyes appeared after 1560 kc.

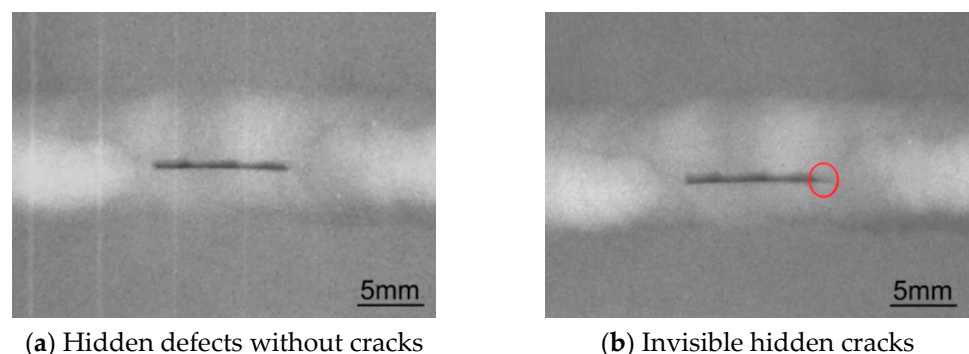


Figure 2. Series photos of X-ray detection for crack evolution.

By referring to X-ray testing results, the tangential signals $H_p(x)$ and normal component signals $H_p(y)$ of different defect levels and their corresponding fatigue cycle numbers are extracted, as shown in Figure 3. The fluctuation of MMM tangent component $H_p(x)$ of hidden crack state is bigger than that of the normal state, although a small jump of $H_p(x)$ occurs on the welded joints in the normal state due to the welding residual stress in Figure 3a. The jump of $H_p(x)$ grows higher when the hidden crack is generated. The value becomes highest when the macroscopic crack is generated. In Figure 3b, the peak-to-peak value of the normal signal component $H_p(y)$ in weld position increases in turn from normal state to hidden crack and then to macroscopic crack, in which the defect levels can be identified by MMM curves. When macroscopic cracks are produced, the polarity varies along the normal component $H_p(y)$ on the SCZs.

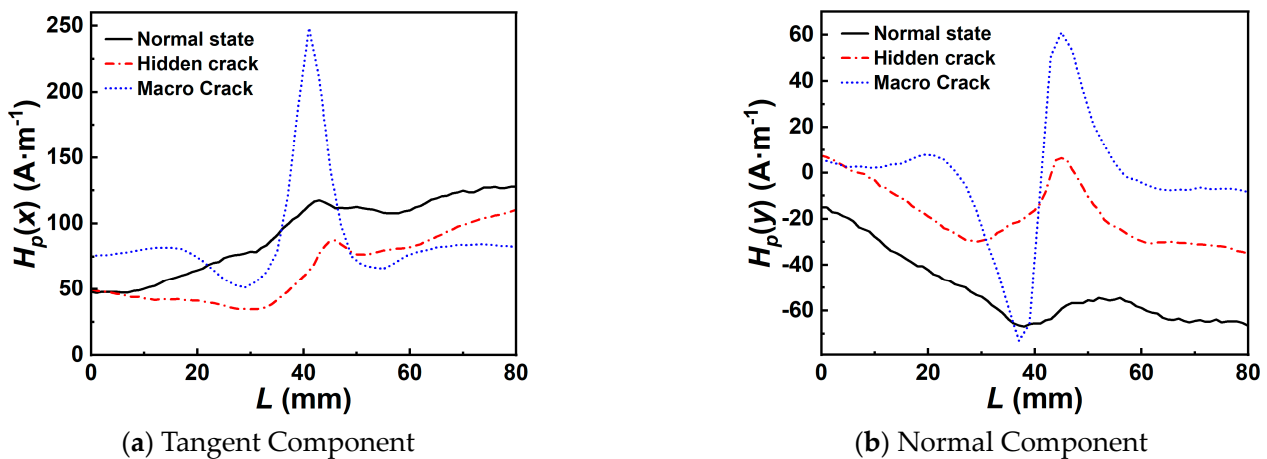


Figure 3. Identifiable defect levels by MMM signals for specimen #55.

Sometimes, due to the interruption of welding residual stress, it is difficult to distinguish between the hidden crack state (1260 kc) and the normal state (0 kc) only by MMM curves shown in Figure 4. The fluctuations of $H_p(x)$ curve in the hidden crack state are very similar to that in the normal state, as shown in Figure 4a. At the same time their curves of $H_p(y)$ overlap with each other in Figure 4b. However, in Figure 5, the result of X-ray detection showed that there was a hidden crack of 1.8 mm on left of the prefabricated defect which has been marked with a circle when the fatigue cycles reach 1260 kc.

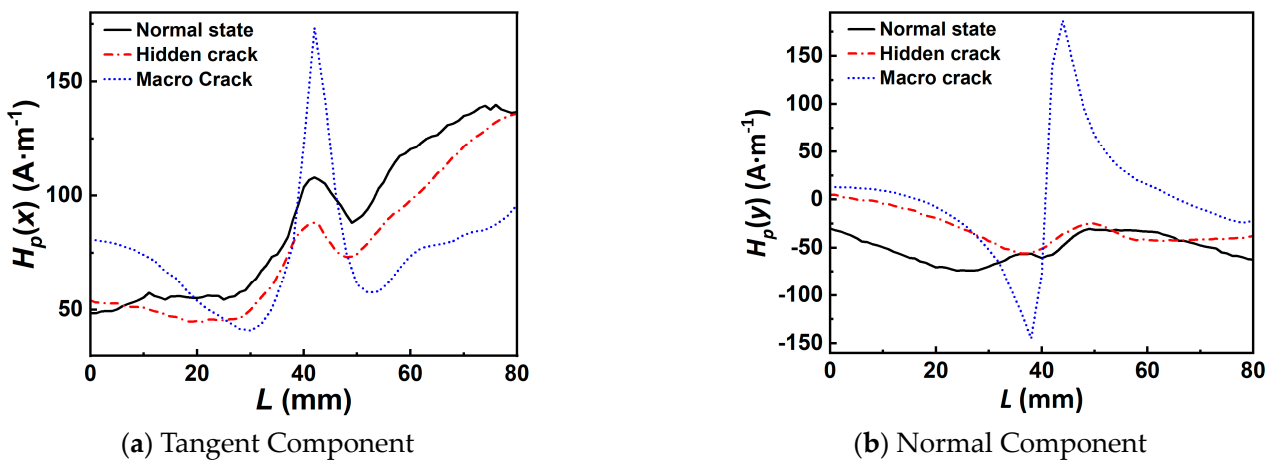


Figure 4. Unidentifiable defect levels by MMM signals for specimen #92.

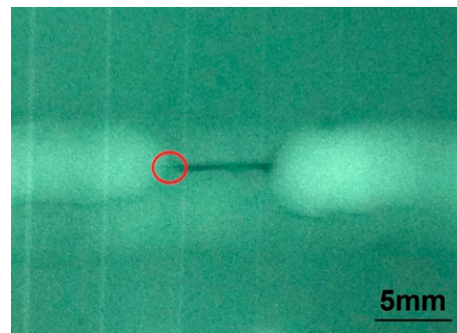


Figure 5. X-ray detection photos of Hidden crack (1260 kc).

4. MLE MMM Modeling

The multiple parameters should be adopted comprehensively because the single MMM characteristic parameter cannot accurately determine the defect levels. For the multiple parameters estimation from the view of mathematical statistics, MLE method is well-suited.

4.1. MLE MMM Modeling

The characteristic parameters of the tangential and normal MMM signals are extracted from the experiment data.

(1) Peak-to-peak value

$$\Delta H_p(x) = H_p^{\max}(x) - H_p^{\min}(x) \quad (1)$$

$$\Delta H_p(y) = H_p^{\max}(y) - H_p^{\min}(y) \quad (2)$$

where $\Delta H_p(x)$ is the tangential peak-to-peak value and $\Delta H_p(y)$ is the normal one. $H_p^{\max}(x)$ and $H_p^{\max}(y)$ are the maximum values of the MMM tangential and normal magnetic induction intensity, respectively. $H_p^{\min}(x)$ and $H_p^{\min}(y)$ are the minimum values of the tangential and normal magnetic induction intensity, respectively.

(2) Gradient

$$G_x = dH_p(x)/dx \quad (3)$$

$$G_y = dH_p(y)/dy \quad (4)$$

where G_x is the tangential gradient, and G_y is the normal one.

(3) Gradient limit state coefficient

$$Z_x = G_x^{\max}/G_x^{\text{ave}} \quad (5)$$

$$Z_y = G_y^{\max}/G_y^{\text{ave}} \quad (6)$$

where Z_x is the tangential gradient limit state coefficient, and Z_y is the normal one. G_x^{\max} and G_x^{ave} are the maximum value and average value of the tangential gradient in the testing zones, respectively. G_y^{\max} and G_y^{ave} are the maximum value and average value of the normal gradient, respectively.

4.2. Kernel Density Function

In order to quantitatively establish the MLE MMM model, the probability density function needs to be built first. X_1, X_2, \dots, X_n are set as independent and identically

distributed random variables in the space R . The probability density function of random variable X in kernel method [23] is defined as:

$$\hat{f} = \frac{1}{nh} \sum_{i=1}^n K\left(\frac{x - x_i}{h}\right) \tag{7}$$

where $K(x)$ is the kernel function, h is the bandwidth, x_i is sample values of X , n is the sample size, and \hat{f} presents the estimated probability density.

The experiment results show that the MMM data obey Gaussian distribution [14], so the Gauss kernel is adopted. The bandwidth h has a great impact on the result of the probability density estimation. If h is too small, the result will be unstable. Otherwise, the resolution ratio of the result is too low. So, the optimized bandwidth algorithm is adopted, which is mainly based on mean integral square error (MISE). Its formula is given in reference [24]. The optimal bandwidth is then calculated by solving the equation with the formula

$$h_{op} = \sqrt[5]{\frac{4nh^6}{\sum_{i=1}^n \sum_{j<i}^n \left[\frac{\sqrt{\pi}}{16h^3} \left\{ [(x_i - x_j)^2 - 6h^2]^2 - 24h^4 \right\} \exp\left(-\frac{(x_i - x_j)^2}{4h^2}\right) \right]}} \tag{8}$$

The iterative algorithm is adopted to find the most optimal bandwidth. First $h_1 = h_{op}(h_0)$ and $h_0 = 1.06\sigma n^{-1/5}$ are calculated, where n is the sample size, σ is the standard deviation of the sample observations. δ is set as a minimum value. When $|h_1 - h_0| > \delta$, cycle steps are performed as follows:

1. Assign the h_1 to the h_0 , that is, $h_0 = h_1$;
2. Bring the new h_0 into $h_1 = h_{op}(h_0)$ to calculate the new h_1 ;
3. $h_1 = (h_0 + h_1)/2$.

According to the above algorithm, the results of the optimized bandwidth are shown in Table 3.

Table 3. Results of optimized bandwidth.

$\Delta H_p(x)$	G_x^{\max}	Z_x^{\max}	$\Delta H_p(y)$	G_y^{\max}	Z_y^{\max}
8.046	1.9236	0.1421	6.9817	1.8659	0.2482

Then, the kernel functions of six MMM characteristic parameters can be obtained, which are $\hat{f}_{\Delta H_p(x)}$, $\hat{f}_{G_x^{\max}}$, $\hat{f}_{Z_x^{\max}}$, $\hat{f}_{\Delta H_p(y)}$, $\hat{f}_{G_y^{\max}}$, $\hat{f}_{Z_y^{\max}}$. These functions form the probability density database of the MMM characteristic parameters. And they are brought into the six kernel density functions to calculate the probability density in the database. The kernel density function is integrated in order to obtain the probability.

4.3. MLE MMM Modeling

The six MMM parameters above contain damage information from different levels. On the basis of the experiment data, these characteristic values are divided into three defect levels, which are normal state, hidden crack state and macroscopic crack state. Considering X-ray detection was taken as the basis comparison of MMM testing experiments, the three defect levels are defined, compared with the current quantitative standards of X-ray detection NB/T 47013.2–2015 and SY/T 4109–2020. In the X-ray detection standards, level I is defined as normal and no defects, level II is defined as the defect length is less than $T/3$, and level III is specified as the defect length is less than $2T/3$, in which T is the nominal thickness of the base metal. The normal state in this paper is consistent with level I of the X-ray detection standard. The hidden crack state, where cracks are invisible to the naked eye and less than 2 mm ($T/3$) in length, is equivalent to level II of the X-ray detection standard. The macroscopic crack state, where cracks are visible to the naked eye and greater

than 2 mm in length, corresponds to level III in the X-ray detection standard. Here, 2 mm only refers to the length of the fatigue crack generated from the end of the prefabricated lack of penetration. The classification standard in this paper is stricter than the X-ray detection standard in order to reflect the advantages of MMM in early damage detection.

From the view of MLE [25], if the total X is discrete, its distribution law is $P\{X = x\} = p(x; \theta)$, $\theta \in \Theta$. Here, θ is the estimated parameter, Θ is the possible range of θ . x_1, x_2, \dots, x_n are set as sample values of X_1, X_2, \dots, X_n . Then, the probability of the incidents $\{X_1 = x_1, X_2 = x_2, \dots, X_n = x_n\}$ is

$$L(\theta) = L(x_1, x_2, \dots, x_n; \theta) = \prod_{i=1}^n p(x_i; \theta), \theta \in \Theta \tag{9}$$

where $L(\theta)$ is the likelihood function.

The MLE estimation models based on MMM characteristic parameters are:

$$L_x = \prod_{i=1}^n p_x(x_i) = p(\Delta H_p(x)) \cdot p(G_x^{\max}) \cdot p(Z_x^{\max}) \tag{10}$$

$$L_y = \prod_{i=1}^n p_y(x_i) = p(\Delta H_p(y)) \cdot p(G_y^{\max}) \cdot p(Z_y^{\max}) \tag{11}$$

where L_x and L_y are the MLE values of the tangential and normal signals, respectively. $p_x(x_i)$ and $p_y(x_i)$ are the probability of x_i based on optimized bandwidth kernel density estimation, respectively.

The MLE probabilities of three defect levels, which are, normal state, hidden crack and macroscopic crack, are shown in Figure 6. The mathematical expectation values of the MLE probability are calculated through mathematical statistics.

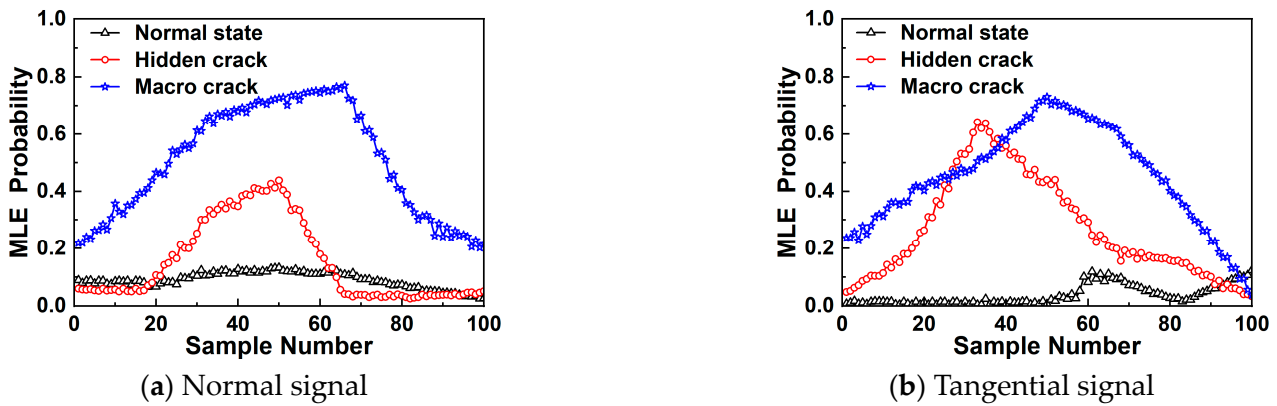


Figure 6. MLE probability of three defect levels.

In this paper, 100 specimens were divided into 10 groups during the fatigue tensile experiments. Each specimen was scanned and the MMM signals were recorded every 20 kilocycles, and 6 characteristic values of each signal curve were extracted. On average, more than 50 sets of data were recorded for each specimen. In total, over 30,000 characteristic values were recorded, along with the corresponding fatigue cycles and defect levels. The Gauss kernel probability density functions of the three defect levels were established based on the database of 30,000 characteristic values. Then, the mathematical expectation values of MLE probability in Table 4 were obtained by integrating the Gauss kernel probability density functions for each defect level.

Table 4. Mathematical expectation of MLE probability.

Mathematical Expectation	Tangential Signal	Normal Signal
Normal state	0.05	0.09
Hidden crack	0.18	0.17
Macroscopic crack	0.41	0.48

It can be seen in Figure 6 that the three damage states can be mostly identified, but there is still partial overlap. Considering that the D–S theory is capable of dealing with uncertain information for small sample data, D–S theory is introduced to modify the above MLE MMM model in order to increase identification accuracy.

5. Modified MLE MMM Model Based on D–S Theory

5.1. MLE Value Neartude

In order to identify the defect levels of welded joints using the D–S evidence theory, the identified framework should be set first. The propositions of the identified framework are the three defect levels which constitute the feature vector. d_{ij} is the distance between MLE probability of the unknown defect level and the mathematical expectation of two MMM signal directions. t_{ij} is proximity. The formulas are as follows:

$$d_{ij} = |A_{ij} - E_j| \tag{12}$$

$$t_{ij} = 1 - \frac{d_{ij}^2}{d_{1j}^2 + d_{2j}^2 + d_{3j}^2} \tag{13}$$

where E_j is an unknown defect level of different MMM signal directions. A_{ij} is the mathematical expectation.

5.2. Reliability Function

Assuming that there is a target to identify, Θ represent all the possible results for the identifying target, and all the possible results are called hypothesis [26]. Θ is set as an identified framework if the set function $m:2^\Theta \rightarrow [0, 1]$ meet the following requirements:

$$m(\varphi) = 0 \tag{14}$$

$$\sum_{A \subset \Theta} m(A) = 1 \tag{15}$$

m is known as the basic reliability allocation (Mass function) of the identified framework. The Formula (14) means no reliability is produced for the empty proposition, and Formula (15) reflects that the sum of all the proposition’s reliability is 1. A is called focal element when $m > 0$ [27]. The $m(A)$ is the basic reliability of subset A , which represents the reliability degree of subset A . For any proposition sets, the reliability function Bel is defined as:

$$Bel(A) = \sum_{B \subset A} m(B) \tag{16}$$

B is an element of subset A . In this paper, subset A is selected as the weld defect level set, and B is the normal state, hidden crack and macroscopic crack.

5.3. Basic Reliability Function Allocation

The basic reliability allocation function m_{ij} and uncertainty $m_j(\Theta)$ of each proposition in the identified framework are as follows:

$$m_{ij} = \frac{t_{ij}}{S - 1} (1 - R_i) \tag{17}$$

$$m_j(\Theta) = R_i \tag{18}$$

where $R_i = b_i \cdot \mu_i$ represents the overall uncertainty whilst identifying the defect level, and μ_i is the uncertainty of MLE probabilities as evidence body in the framework, which can be given by expert opinion or data statistics of the experiment, 0.1 is taken. $S = 3$ represents three defect levels.

$$b_i = \sqrt{\frac{1}{2} \sum_{\substack{j=1 \\ j \neq m}}^3 (t_{ij} - u_i)^2} \tag{19}$$

$$u_i = \frac{1}{2} \sum_{\substack{j=1 \\ j \neq m}}^3 t_{ij} \tag{20}$$

where b_i is the variance of the proximity except for the biggest proximity of the proposition close to the unknown defect level. And u_i is the mean value of the proximity except for the biggest proximity of the proposition that is close to the unknown defect level.

5.4. D–S Information Fusion

(1) Two Reliability Functions Fusion

Bel_1 and Bel_2 are two reliability functions of the same target framework set, m_1 and m_2 are the basic reliability allocation of function Bel_1 and Bel_2 , respectively. MLE probabilities of the tangential and normal MMM characteristic value are selected as the Bel_1 and Bel_2 . C and D represent the defect levels of tangential and normal signals, respectively.

$$\sum_{C_i \cap D_j = \varnothing} m_1(C_i)m_2(D_j) < 1 \tag{21}$$

Then, the basic reliability allocation is:

$$m(C) = \begin{cases} 0 & C = \varnothing \\ \frac{\sum_{C_i \cap D_j = C} m_1(C_i)m_2(D_j)}{1-k} & C \neq \varnothing \end{cases} \tag{22}$$

$$k = \left(\sum_{C_i \cap D_j = \varnothing} m_1(C_i)m_2(D_j) \right) \tag{23}$$

where k represents the inconsistency factor. $i, j = 1, 2, 3$ represent the level of defect levels, which are: 1 is normal state, 2 is hidden crack state and 3 is macroscopic crack state.

(2) Decision rules of D–S theory

$$m(C_1) = \max(m(C_i), C \subset \Theta) \tag{24}$$

$$m(C_2) = \max(m(C_i), C \subset \Theta, C_i \neq C_1) \tag{25}$$

$$\begin{cases} m(C_1) - m(C_2) > \varepsilon_1 \\ m(\Theta) < \varepsilon_2 \\ m(C_1) > m(\Theta) \end{cases} \tag{26}$$

The recognition result is C_1 when meeting the conditions of Formulas (24) to (26), where $m(\Theta)$ is the uncertainty degree, and ε_1 and ε_2 are set as threshold value.

6. Validation

Under the same experimental conditions, thirty specimens of unknown weld defect levels had been selected to verify the modified MLE MMM model based on the D-S theory. Take specimen 17 as an example, after 980 fatigue kilocycles, the specimen, which showed no macroscopic crack visible to the naked eye, was examined by X-rays. The result of X-ray detection showed that there were no hidden cracks on both sides of the prefabricated defect shown in Figure 7.



Figure 7. Result of X-ray detection of specimen 17#.

Then, by analyzing the MMM data, the tangential and normal components of ΔH_p , G and Z are (28.9, 5.75, 2.441) and (9.6, 6.5, 5.007), respectively. Then, the tangential and normal MLE probabilities are calculated, respectively, by Formulas (10) and (11), the results are 0.16 and 0.12. The proximity of the unknown defect level are obtained by Formulas (12) and (13), and the results are listed in Table 5. Then, the basic reliability allocation is calculated by Formulas (17) and (18), shown in Table 6.

Table 5. MLE probability proximity of the identifying damage state.

Proximity	Tangential Signal	Normal Signal
Normal state	0.84	0.99
Hidden crack	0.99	0.98
Macroscopic crack	0.17	0.03

Table 6. Basic reliability allocation of the identifying damage state.

Basic Reliability Allocation	Tangential Signal	Normal Signal
Normal state	0.47	0.41
Hidden crack	0.47	0.48
Macroscopic crack	0.01	0.08
Uncertainty degree	0.047	0.033

It can be seen that the basic reliability allocations of the normal and hidden crack are similar. It is still difficult to identify the unknown defect level only based on the basic reliability allocation. So, it is necessary to use the information fusion. The information fusion results are listed in Table 7.

Table 7. Information fusion results.

	$m_{bel1} = D_1(0.41)$	$m_{bel1} = D_2(0.48)$	$m_{bel1} = D_3(0.08)$	$m_{bel1} = \Theta(0.033)$
$m_{bel2} = C_1(0.47)$	$C_1(0.1927)$	$\Phi(0.2256)$	$\Phi(0.0376)$	$C_1(0.01551)$
$m_{bel2} = C_2(0.47)$	$\Phi(0.1927)$	$C_2(0.2256)$	$\Phi(0.0376)$	$C_2(0.01551)$
$m_{bel2} = C_3(0.01)$	$\Phi(0.0041)$	$\Phi(0.0048)$	$C_3(0.0008)$	$C_3(0.00033)$
$m_{bel2} = \Theta(0.047)$	$C_1(0.01927)$	$C_2(0.02256)$	$C_3(0.00376)$	$\Theta(0.00155)$

The inconsistency factor k is calculated by Formula (23), and the result is as follows:

$$k = 0.2256 + 0.04 + 0.0376 + 0.1458 + 0.1927 + 0.0376 + 0.0041 + 0.0048 = 0.5024$$

So, the basic reliability allocation of the evidence Bel_1 and Bel_2 is calculated by Formula (22). And the reliability allocation after information fusion is shown in Table 8.

Table 8. Reliability allocation of information fusion.

Reliability	m (Tangential Normal)
Normal state	0.46
Hidden crack	0.53
Macroscopic crack	0.0098
$m_j(\Theta)$	0.003

According to the decision rules of the D–S theory, ε_1 and ε_2 are taken as 0.01 and 0.001, then the prediction result is hidden crack. The results show the reliability is 53% and uncertainty degree $m(\Theta)$ is 0.3%.

In order to determine the unknown defect level from the experimental point of view, a scanning electron microscopy (SEM) has been applied to test the selected specimen. At the end of the prefabricated defect, the wire-electrode cutting was used to obtain the SEM specimen as shown in the dashed box in Figure 8. The cutting surface 1 is the SEM observation surface with the length of 15 mm. The distance from the cutting surface 2 to 1 was 10 mm.

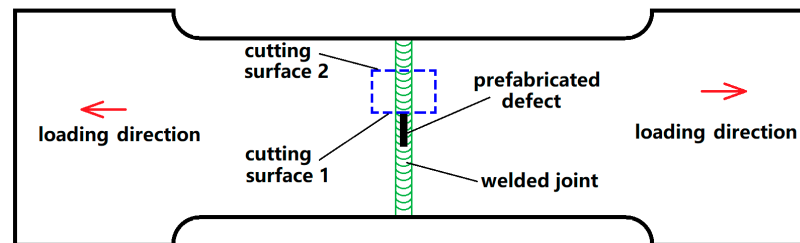


Figure 8. SEM unit acquisition program.

The SEM result is shown in Figure 9. Some hidden cracks circled by ellipses with a size of about 0.25 mm have appeared in Figure 9. This result is consistent with the predictions of the modified MLE MMM model, which shows that the modified MLE MMM model can identify hidden crack damage earlier than X-ray detection. The other 29 specimens have the same verification process as specimen 17. The smallest uncertainty degree is 0.30%, the largest one is 7.09%, and the average one is 3.66%, as shown in Figure 10. The results verify the validity of the modified MLE MMM model based on the D–S theory.

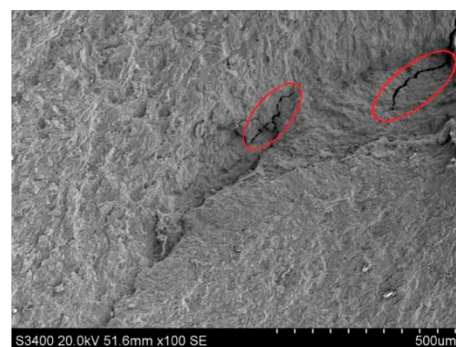


Figure 9. Scanning electron microscope along cutting surface 1, photo showing two hidden cracks on specimen 17#.

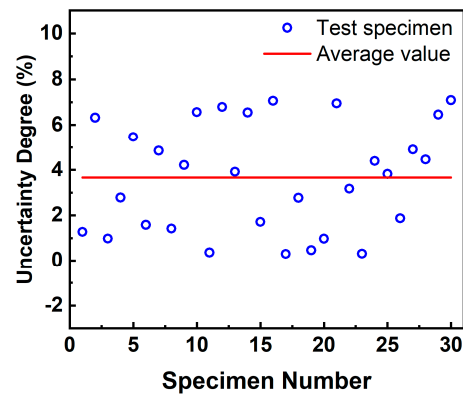


Figure 10. Uncertainty degrees of the verification specimens.

7. Conclusions

(1) Due to the existence of welding residual stress, it is difficult to distinguish between the normal state and the hidden crack state. At the same time, considering that a single MMM feature parameter cannot accurately reflect the level of welding defects, it is necessary to extract multiple MMM feature parameters, namely $\Delta H_p(x)$, G_x^{\max} , Z_x^{\max} , $\Delta H_p(y)$, G_y^{\max} and Z_y^{\max} for quantitative identification;

(2) The different defect levels, that is, normal state, hidden crack and macroscopic crack, can be identified based on the MLE MMM model from mathematical statistics. But there exists a partial overlap between normal state and hidden crack state. So, the modified MLE MMM model based on the D–S theory is presented, of which the smallest uncertainty degree is 0.3%, the largest one is 7.09%, and the average one is 3.66%;

(3) The validation results are consistent with the prediction result of the modified MLE MMM model based on D–S theory. It shows that the modified model is effective in distinguishing early hidden cracks from welding residual stress, which is earlier than X-ray detection. The method is suitable for ferromagnetic materials such as Q235B and Q345. This provides a new tool of MMM quantitative identification for weld defect levels.

Author Contributions: Conceptualization, H.X.; methodology, C.X.; software, S.G.; investigation, M.Y.; resources, H.X.; writing—original draft preparation, H.X. and C.X.; writing—review and editing, H.X. and C.X.; supervision, H.X.; Formal analysis, W.L. All authors have read and agreed to the published version of the manuscript.

Funding: This research was funded by the Natural Science Foundation of Heilongjiang Province of China (Grant No. LH2019A004) and the National Natural Science Foundation of China (Grant No. 11272084).

Institutional Review Board Statement: Not applicable.

Informed Consent Statement: Not applicable.

Data Availability Statement: Not applicable.

Acknowledgments: The authors would like to thank the referees for their helpful comments and suggestions.

Conflicts of Interest: The authors declare no conflict of interest.

References

- Jambor, M.; Pokorny, P.; Trsko, L.; Oplt, T.; Jackova, M.; Hutar, P. Microstructure and the fatigue crack propagation in the dissimilar low alloy/stainless steel GMAW welded joints. *Mater. Charact.* **2022**, *191*, 112119. [[CrossRef](#)]
- Wang, X.J.; Meng, Q.C.; Hu, W.P. Fatigue life prediction for butt-welded joints considering weld-induced residual stresses and initial damage, relaxation of residual stress, and elasto-plastic fatigue damage. *Fatigue Fract. Eng. Mater. Struct.* **2019**, *42*, 1373–1386. [[CrossRef](#)]
- Su, S.Q.; Yang, Y.Y.; Wang, W.; Ma, X.P. Crack propagation characterization and statistical evaluation of fatigue life for locally corroded bridge steel based on metal magnetic memory method. *J. Magn. Magn. Mater.* **2021**, *536*, 168136. [[CrossRef](#)]

4. Bao, S.; Jin, P.F.; Zhao, Z.Y.; Fu, M.L. A Review of the Metal Magnetic Memory Method. *J. Nondestruct. Eval.* **2020**, *39*, 11. [[CrossRef](#)]
5. Moonesan, M.; Kashefi, M. Effect of Sample Initial Magnetic Field on the Metal Magnetic Memory NDT Result. *J. Magn. Magn. Mater.* **2018**, *460*, 285–291. [[CrossRef](#)]
6. Ozhigov, L.S.; Mitrofanov, A.S.; Dobrovol'skaya, I.Y.; Shramchenko, S.V.; Vasilenko, R.L.; Rybal'chenko, N.D.; Krainyuk, E.A. Corrosion Defects in Pipelines of Nuclear Power Plants and the Problems of Their Inspection. *Mater. Sci.* **2018**, *53*, 777–782. [[CrossRef](#)]
7. Wang, H.P.; Dong, L.H.; Wang, H.D.; Ma, G.Z.; Xu, B.S.; Zhao, Y.C. Effect of tensile stress on metal magnetic memory signals during on-line measurement in ferromagnetic steel. *NDT E Int.* **2020**, *117*, 102378. [[CrossRef](#)]
8. Kashefi, M.; Clapham, L.; Krause, T.W.; Underhill, P.R.; Krause, A.K. Stress-Induced Self-Magnetic Flux Leakage at Stress Concentration Zone. *IEEE Trans. Magn.* **2021**, *57*, 6200808. [[CrossRef](#)]
9. Dubov, A.; Dubov, A.; Kolokolnikov, S. Detection of local stress concentration zones in engineering products—the lacking link in the non-destructive testing system. *Weld. World* **2018**, *62*, 301–309. [[CrossRef](#)]
10. Shi, P.P.; Hao, S. Analytical solution of magneto-mechanical magnetic dipole model for metal magnetic memory method. *Acta Phys. Sin.* **2021**, *70*, 034101. [[CrossRef](#)]
11. Avakian, A.; Ricoeur, A. An extended constitutive model for nonlinear reversible ferromagnetic behaviour under magnetomechanical multiaxial loading conditions. *J. Appl. Phys.* **2017**, *121*, 053901. [[CrossRef](#)]
12. Ni, C.; Hua, L.; Wang, X.K. Crack propagation analysis and fatigue life prediction for structural alloy steel based on metal magnetic memory testing. *J. Magn. Magn. Mater.* **2018**, *462*, 144–152. [[CrossRef](#)]
13. Yao, K.; Wu, L.B.; Wang, Y.S. Nondestructive Evaluation of Contact Damage of Ferromagnetic Materials Based on Metal Magnetic Memory Method. *Exp. Tech.* **2019**, *43*, 273–285. [[CrossRef](#)]
14. Xu, K.S.; Yang, K.; Liu, J.; Wang, Y. Study on metal magnetic memory signal of buried defect in fracture process. *J. Magn. Magn. Mater.* **2020**, *498*, 166139. [[CrossRef](#)]
15. Liu, B.; Lian, Z.; Liu, T.; Wu, Z.H.; Ge, Q. Study of MFL signal identification in pipelines based on non-uniform magnetic charge distribution patterns. *Meas. Sci. Technol.* **2023**, *34*, 044003. [[CrossRef](#)]
16. Liu, B.; Luo, N.; Feng, G. Quantitative Study on MFL Signal of Pipeline Composite Defect Based on Improved Magnetic Charge Model. *Sensors* **2021**, *21*, 3412. [[CrossRef](#)]
17. Xing, H.Y.; Dang, Y.B.; Wang, B.; Leng, J.C. Quantitative Metal Magnetic Memory Reliability Modeling for Welded Joints. *Chin. J. Mech. Eng.* **2016**, *29*, 372–377. [[CrossRef](#)]
18. Xing, H.Y.; Xu, C.; Liu, C. Characterization of Physical Short Crack Growth at the Meso-scale Based on Magnetic Property Parameters. *Adv. Eng. Sci.* **2023**, *55*, 307–314. [[CrossRef](#)]
19. *JB/T 4730-2005*; Nondestructive Testing of Pressure Equipments. Xinhua Publishing House of China: Beijing, China, 2010.
20. Ren, S.K.; Ren, X.Z.; Duan, Z.X.; Fu, Y.W. Studies on influences of initial magnetization state on metal magnetic memory signal. *NDT E Int.* **2019**, *103*, 77–83. [[CrossRef](#)]
21. Chen, H.L.; Wang, C.L.; Zuo, X.Z. Research on methods of defect classification based on metal magnetic memory. *NDT E Int.* **2017**, *92*, 82–87. [[CrossRef](#)]
22. *GB/T 3075-2008*; Metallic Materials—Fatigue Testing—Axial-Force-Controlled Method. Standards Press of China: Beijing, China, 2010.
23. Arora, S.; Taylor, J.W. Forecasting electricity smart meter data using conditional kernel density estimation. *Omega-Int. J. Manag. Sci.* **2016**, *59*, 47–59. [[CrossRef](#)]
24. Davies, T.M.; Baddeley, A. Fast computation of spatially adaptive kernel estimates. *Stat. Comput.* **2018**, *28*, 937–956. [[CrossRef](#)]
25. Yamamura, K. Bayes estimates as an approximation to maximum likelihood estimates. *Popul. Ecol.* **2016**, *58*, 45–52. [[CrossRef](#)]
26. Can, C.E.; Ergun, G.; Soyer, R. Bayesian Analysis of Proportions via a Hidden Markov Model. *Methodol. Comput. Appl. Probab.* **2022**, *24*, 3121–3139. [[CrossRef](#)]
27. Cao, L.X.; Liu, J.; Han, X.; Jiang, C.; Liu, Q.M. An efficient evidence-based reliability analysis method via piecewise hyperplane approximation of limit state function. *Struct. Multidiscip. Optim.* **2018**, *58*, 201–213. [[CrossRef](#)]

Disclaimer/Publisher's Note: The statements, opinions and data contained in all publications are solely those of the individual author(s) and contributor(s) and not of MDPI and/or the editor(s). MDPI and/or the editor(s) disclaim responsibility for any injury to people or property resulting from any ideas, methods, instructions or products referred to in the content.